sciendo ARTIFICIAL SATELLITES, Vol. 58, No. 2 – 2023
DOI: 10.2478/arsa-2023-0006

SIMILARITIES AND DIFFERENCES IN THE EARTH'S WATER VARIATIONS SIGNAL PROVIDED BY GRACE AND AMSR-E OBSERVATIONS USING MAXIMUM COVARIANCE ANALYSIS AT VARIOUS LAND COVER DATA BACKGROUNDS

Viktor SZABÓ, Katarzyna OSIŃSKA-SKOTAK

Warsaw University of Technology, Faculty of Geodesy and Cartography, Warsaw, Poland

e-mails: viktor.szabo.dokt@pw.edu.pl, katarzyna.osinska-skotak@pw.edu.pl

ABSTRACT. The study presents a compatibility analysis of gravimetric observations with passive microwave observations. Monitoring the variability of soil water content is one of the essential issues in climate-related research. Total water storage changes (ΔTWS) observed by Gravity Recovery and Climate Experiment (GRACE), enables the creation of many applications in hydrological monitoring. Soil moisture (SM) is a critical variable in hydrological studies. Advanced Microwave Scanning Radiometer (AMSR-E) satellite products provided unique observations on this variable in near-daily time resolutions. The study used maximum covariance analysis (MCA) to extract principal components for ΔTWS and SM signals. The analysis was carried out for the global area, dividing the discussion into individual continents. The amplitudes of gravimetric and microwave signals were computed via the complex empirical orthogonal function (EOF) and the complex conjugate EOF* to determine the regions for detailed comparison. Similarities and differences in signal convergence results were compared with land cover data describing soil conditions, vegetation cover, urbanization status, and cultivated land. Convergence was determined using Pearson correlation coefficients and cross-correlation. In order to compare ΔTWS and SM in individual seasons, ΔTWS observations were normalized. Results show that naturally forested areas and large open spaces used for agriculture support the compatibility between GRACE and AMSRE observations and are characterized by a good Pearson correlation coefficient >0.8. Subpolar regions with permafrost present constraints for AMSR-E observations and have little convergence with GRACE observations.

Keywords: GRACE, AMSR-E, total water storage anomalies, soil moisture, remote sensors

1. INTRODUCTION

Soil moisture (SM) is a critical hydrologic state variable of the land that crosses the interfaces of several disciplines, of significant importance for numerous applications for meteorology, hydrology, climatology, and ecology (Robinson et al., 2008). Small changes in gravity measured from space also deduced water mass fluctuations. Launched in March 2002 twin-satellite system Gravity Recovery and Climate Experiment (GRACE) (Tapley et al., 2004b) and GRACE Follow-On (GRACE-FO) (Flechtner et al., 2016) provided unique information regarding gravity changes caused by the mass transport over the Earth's surface. Changes in total water storage

(ΔTWS) (Wahr et al., 1998) show the Earth's mass change on a near-monthly timescale. The derivative of the TWS signal is TWS anomaly (TWSA), understood as a combined monthly averaged water storage change by removing the long-term average divided by standard deviation. TWSA corresponds to the sum of all above and below surface water storage, including SM, canopy water, lakes, rivers, and groundwater. The importance of SM and ΔTWS for understanding the Earth's water cycle, and the factors affecting it over the years, has been considered in many studies individually.

The influence of estimating spatial and temporal variations of SM on climate changes was described in multiple studies (Betts et al., 1994, Engman, 1992, Entekhabi et al., 1994, Fast and McCorcle, 1991, Jackson et al., 1987, Petropoulos et al., 2014, Saha, 1995, Topp et al., 1980). Spatial and temporal variability of water was well documented in previous work for SM (Crow et al., 2012, Famiglietti et al., 2008, Vereecken et al., 2014) and ΔTWS (Landerer and Swenson, 2012, Tapley et al., 2004a, Zhao et al., 2017). From a hydrological point of view, analysis of spatiotemporal patterns of SM and ΔTWS observations is essential to understanding their behavior. In literature, existing methods describe variability only in the spatial domain (Haining et al., 2010, Khaki et al., 2017) or only in the temporal domain, based on time series analysis (Fu, 2011, Sprott and Sprott, 2003, Vishwakarma et al., 2021). Several methods can be found in the literature that analyzes ΔTWS and SM space and time domains together such as temporal stability analysis (TSA) (Martínez-Fernández and Ceballos, 2005, Wang et al., 2018), triple collocation (TC) (Crow et al., 2015, Gruber et al., 2017, Hasan and Tarhule, 2021, Yin and Park, 2021), and empirical orthogonal functions (EOFs) (Eom et al., 2017, Lei et al., 2012, Navarra and Simoncini, 2010, Schrama et al., 2007, Yoo and Kim, 2004). Whether the analysis is temporal or spatiotemporal, researchers in previous work have indicated the importance of SM as a component of the ΔTWS signal.

Water content in near-surface soil layers is a significant component of the ΔTWS signal observed by the GRACE mission. There have been many significant studies examining the relationship between SM and ΔTWS. A joint comparison of the remote sensing retrieval products' metric entropy and fluctuation complexity was considered in (Kumar et al., 2018). The satellite products of Advanced Microwave Scanning Radiometer (AMSR-E), Advanced Scatterometer (ASCAT), Soil Moisture and Ocean Salinity (SMOS), and Advanced Microwave Scanning Radiometer 2 (AMSR2) show significant noise (high entropy, low complexity), except Soil Moisture Active Passive (SMAP) is slightly noisy and more informative. The correlation greater than 0.7 between TWSA and SM data was shown in previous work (Abelen and Seitz, 2013, Crow et al., 2017, Swenson et al., 2008b). Expanding the shallow groundwater variation under the SM root zone is an essential issue in scientific research. Since using microwave satellites may be a possible way to isolate groundwater storage (GWS) variations from the GRACE signal (Frappart and Ramillien, 2018, Yeh et al., 2006), a significant area of research is the possibility of using microwave observations to determine SM.

Microwave remote sensing observations have been applied for the determination of SM (Babaeian et al., 2019). Active and passive microwave remote sensing provides an observation of SM at global and regional scales (Bartalis et al., 2007, Chen et al., 2018, Jackson et al., 2010, Kerr et al., 2016, Koike et al., 2004, Ulaby, 1982, Vinnikov et al., 1999, Wagner et al., 2013). It helps in much scientific research in hydrology and climate studies and gives an opportunity to understand environmental changes (Njoku and Entekhabi, 1996). GRACE ΔTWS and remote sensing microwave SM observations have recently been used to improve SM and GWS simulations (Tangdamrongsub et al., 2022, Tian et al., 2017).

One of the essential microwave sensors providing SM data was the AMSR-E mission. Owing to the long joint period in orbit during the operation of GRACE and AMSR-E missions, numerous previous studies have considered comparing SM from AMSR-E and ΔTWS signals from these sensors. Comparisons between the AMSR-E surface wetness index (ASWI) and the GRACE drought severity index (DSI) were shown in the previous work (Du et al., 2019). The indicated comparisons showed robust correlations in regions in the United States (R higher than 0.7 for 29 percent of the area) during the summer months (June–August) from 2002 to 2017 for regions where a semiannual temporal lag between fast surface water changes and the slower GWST was considered. The study explores multivariate data assimilation (DA) using synthetic ΔTWS from GRACE and synthetic AMSR-E passive microwave brightness temperature spectral differences (dTb) in case estimation of snow water equivalent (SWE) over snow-covered terrain was presented by Wang et al. (2021) and Wang and Forman (2020). In a previous study (Seo et al., 2010), the authors propose methods to estimate solid precipitation accumulation in winter in the northern Arctic region. Based on the GRACE and AMSR-E, winter season solid precipitation accumulation was estimated. In the second step, estimated values was compared with the traditional estimations from the Global Precipitation Climatology Project (GPCP) and Climate Prediction Center's Merged Analysis of Precipitation (CMAP). Correlation, time shift, and principal component analyses of SM from the WaterGAP Global Hydrology Model (WGHM) and the satellite sensors AMSR-E and ASCAT to total water storage variations from the satellite gravity mission GRACE in the area of the La Plata Basin in South America were provided by Abelen et al. (2015). Regional and global variations in SM from satellite sensor AMSR-E and GRACE was also considered in Abelen et al. (2011). Global Land Data Assimilation System (GLDAS) (Rodell et al., 2004) product was used to evaluate AMSR-E observations over central Tibetan Plateau (Chen et al., 2013). To effectively catch drought disasters in the Guangdong province of southern China in 2004–2005, 2007, and 2009 SM from AMSR-E was used (Chen et al., 2012). The highest SM variability in the surface soil layer can be observed because of meteorological and environmental interactions such as precipitation, temperature changes, porosity, topography, vegetation processes, and human factors.

Although many studies have been performed on evaluating extreme hydrological events using GRACE and AMSR-E, there is a gap in the published literature concerning ΔTWS and SM signal convergence considering land cover data described soil conditions, vegetation cover, urbanization status, and cultivated land. Since the information collected by gravimetric sensors has a lower temporal frequency and spatial resolution than microwave measurements, it is crucial to investigate the convergence of these signals. The key question posed in the article is: is it possible to use the information contained by sensors characterized by higher noise and signal variance, such as AMSR-E, in the global analysis of ΔTWS variability from GRACE satellites? In work, it was decided to present the similarities and differences in the Earth's water resource measurements. This article analyzes the spatiotemporal variations of SM and ΔTWS in the context of the similarity pattern comparison. The study used maximum covariance analysis (MCA) to extract principal components for ΔTWS and SM signals.

2. DATA AND METHODS

2.1. Data

GRACE data is available at https://podaac-tools.jpl.nasa.gov/(accessed on 01.06.2022) distributed by the Center for Space Research (CSR). The spatial resolution of the GRACE data included in the study is approximately 300 km x 300 km. Surface and subsurface mass change data are based on the RL06 standards (Dahle et al., 2013) at the L2 data processing level. Processing GRACE data included replaced coefficient C_{20} representing gravimetric flattening of the Earth (Swenson et al., 2008a) by Satellite Laser Ranging (SLR) observation (Cheng and Tapley, 2004) and filtered out the correlated error (Swenson and Wahr, 2006) using a modified de-correlation filter (Chen et al., 2007). Processing GRACE data also included excluding the static part of the gravity field using GGM05C model (Ries et al., 2016). During processing GRACE data the degree-1 coefficients (Geocenter) are estimated using the methods from Sun et al. (2016) and Swenson et al. (2008b). A glacial isostatic adjustment (GIA) correction has been applied based on the ICE6G-D model from Peltier et al. (2018).

The Advanced Microwave Scanning Radiometer for the Earth Observing System is a passive multiband sensor of NASA's Earth Observing System Aqua satellite. AMSR-E uses the X-band and C-band to measure the water cycle and SM content retrievals corresponding to the depth of (2.5–3.75cm) and (3.75–7.5cm), respectively. Owing to the fact that radio frequency interference (RFI) in the C-band (6.9 and 10.7 GHz), the X-band has been extensively used for SM retrieval (Njoku et al., 2005). AMSR-E dataset is available as daily files at https://disc.gsfc.nasa.gov/(accessed on 01.06.2022). AMSR-E/Aqua surface SM ascending V002 is a Level 3 (gridded) data set with a daily frequency and spatial resolution of about 25 km by 25 km. Land surface SM measurements is derived from passive microwave remote sensing data using the Land Parameter Retrieval Model (LPRM). The LPRM is based on a forward radiative transfer model to retrieve surface SM and vegetation optical depth. The dataset contains data from May 2002 to December 2011. AMSR-E on the NASA EOS Aqua satellite discontinued producing data in October 2011 due to an issue with the rotation of its antenna (van der Vliet et al., 2020). Only descending tracks were used because of the much better stability of nighttime soil, canopy, and air temperatures in this study (De Jeu et al., 2008, Draper et al., 2009, Liu et al., 2012, 2011, Owe et al., 2001).

The intersection of the GRACE and AMSR-E sensors datasets was selected for analysis. The time range of the selected data for this study was chosen to cover the maximum part intersection of existing GRACE and AMSR-E datasets. The dataset in the analysis contains data from 2002 to 2012 from both missions.

2.2. Methodology

Data preparation involved averaging with moving window data collected by the AMSR-E sensor over the GRACE epochs. As the compared sensors have different spatial resolutions, the data from AMSR-E were linearly interpolated on the GRACE resolution. The values for ΔTWS observed by GRACE and AMSR-E have different amplitudes. To be able to compare these results to each other, it was decided to normalize data for each season and then compare the normalized values for given seasons to minimize the effects of seasonality. Volumetric soil water content collected by AMSR-E sensor is the volume of water per unit volume of soil $[m^3_{water}/m^3_{soil}]$ (Njoku et al., 2003). Volumetric water content (VSM) can be expressed as a ratio, percentage, or depth of water per soil (assuming a unit surface area). As the VSM data from ARMS-E were already presented as percentages, normalization was provided only at ΔTWS from GRACE. Since results of retrieving global surface SM from GRACE depend on used SM extreme values, the authors of Sadeghi et al. (2020) proposed used extreme values from overlapping SMAP and GRACE timelines from 2015 to 2017. This research used maximum and minimum values from the overlapping periods of GRACE and AMSR-E from 2002 to 2011. Normalization was performed according to the following equation:

$$TWS_{norm} = \frac{TWS - TWS_{min}}{TWS_{max} - TWS_{min}} \tag{1}$$

To reveal the similarities and differences between the values, both sensor signals were grouped for the winter, spring, summer, and autumn months. Moreover, a complementary correlation analysis was performed to assess the level of agreement between different data sources:

$$corr_{(tws),(sm)} = \frac{\sum_{i=1}^{n}(TWS_i - \mu_{tws})(SM_i - \mu_{sm})}{\sqrt{\sum_{i=1}^{n}(TWS_i - \mu_{tws})^2(SM_i - \mu_{sm})^2}} \tag{2}$$

where μ is the mean value, and σ its standard deviation. However, some phase shifts are observed between the signals in the selected values delivered by analyzed sensors. Therefore, the analysis of signal similarity was completed with the normalized cross-correlation $(xcorr)$ coefficients:

$$xcorr_{tws(t),sm(t+\tau)} = \frac{E[(TWS_t - \mu_{tws})\overline{(SM_{t+\tau} - \mu_{sm})}]}{\sigma_{tws}\sigma_{sm}} \tag{3}$$

where E is the expected value of the given expression and τ is the time shift. In this case, a maximum 6 months interval of possible lags between the examined time series was determined. Anomalies for SM were also determined to indicate the similarities and differences with TWSA resulting from extreme environmental changes. TWSA and SM anomalies (SMA) were calculated by the following equations:

$$SMA_{(t)} = \frac{SM_{(t)} - \mu_{sm}}{\sigma_{sm}} \tag{4}$$

$$TWSA_{(t)} = \frac{TWS_{(t)} - \mu_{tws}}{\sigma_{tws}} \tag{5}$$

Intense spatial averaging filters with a high radius of smoothing kernel can cause signal loss, known as "leakage error" (Longuevergne et al., 2010, Swenson and Wahr, 2002). Filtering decreases the spatial resolution of the GRACE observation, making it challenging to identify the mass water signal of the main stem. The EOF analysis is a method for GRACE data to separate signals from signal noise. It is beneficial in cases such as problems with loss of geophysical signal with diminishing spatial resolution during filtration (Wouters and Schrama, 2007). The use of this method is justified in the case of comparison of microwave data with higher spatial resolution and greater time frequency of measurements than gravimetric satellite measurements. Concerning the EOF's of standard MCA (Rieger et al., 2021), the spatial amplitude (As) provides a means to understand which regions contribute the most to the given mode. The spatial amplitude is easily computed via the complex EOF and the complex conjugate EOF*:

$$As = \sqrt[2]{EOF \times EOF^*} \in \mathbb{C} \tag{6}$$

We can determine exactly how the individual regions are dynamically linked to each other. Phase shifts between these two cases are signals that can be combined into one mode with standard MCA by the following equation:

$$\theta = \tan(\frac{\mathbb{R}(EOF)}{\mathbb{I}(EOF)})^{-1} \tag{7}$$

3. RESULTS

The surface soil layer commonly shows the most considerable SM variability due to the relations with meteorological, environmental, and anthropogenic factors such as porosity, topography, vegetation, precipitation, and temperature decreasing with depth. To analyze land cover conditions, the Harmonized World Soil Database was used (Fischer et al., 2008) from https://www.fao.org/soils-portal/data-hub/(accessed on 01.06.2022). Land cover data contain datasets based on an iterative calculation procedure to estimate land cover class weights. It was consistent with combined Food and Agriculture Organization (FAO) land statistics and spatial land cover characteristics. Data was collected from remote sensing data, allowing intepretation and classification of land cover shares in 5' by 5' latitude/longitude grid cells. The class weights used in the study determine the presence of arable land and forests for each land cover class. As the water content strongly depends on the soil porosity, the analysis included classes presenting soil conditions in terms of oxygen content.

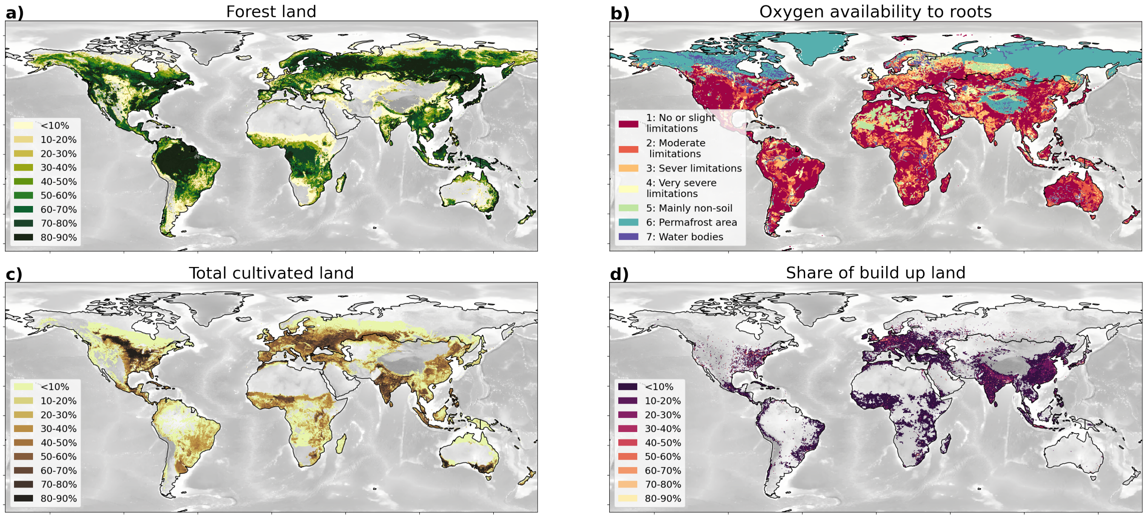

Figure 1. Land cover data of forest land (a), oxygen availability to roots (b), total cultivated land (c), and share of build-up land (d) based on Harmonized World Soil Database

Drainage characteristics of soils broadly define oxygen availability in soils. The determination of soil drainage classes is based on procedures developed at FAO. These procedures consider soil type, texture, terrain slope, and phases with mean proportion of water, air, and solids in soil. This publication contains characteristics of forest land, oxygen availability to roots, total cultivated land, and share of build-up land in Figure 1.

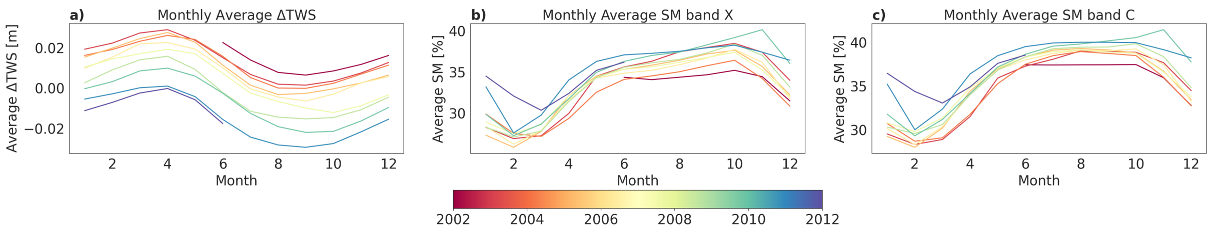

Figure 2. Seasonal patterns of ∆TWS (a), SM from band X (b), and SM from band C (c) grouped by month over time

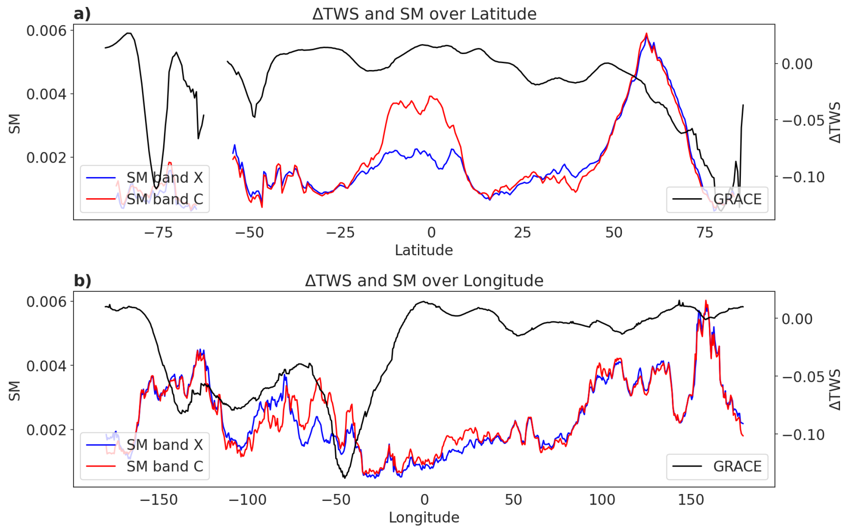

Figure 3. Average SM from AMSR-E and ΔTWS from GRACE grouped by latitude (a) and longitude (b)

The SM and ΔTWS variables are characterized by high variability over time. The main components are related to seasonal factors included and the occurrence of dry and rainy seasons. This decline over the years is presented in Figure 2. The figure clearly shows the negative trend of ΔTWS value over the years. There are no similarities between the averaged SM and ΔTWS observations for a given month. Since the cyclic signal can be reset by cyclical phenomena occurring in a given area, the article presents averaged anomalies concerning time and latitude.

In order to characterize the values collected by gravimetric and microwave sensors, the averaged values of the observation epochs in the years 2002–2011 were determined concerning the latitude and longitude, respectively, as shown in Figure 3. Mean anomalies and standard deviation of anomalies in time over the latitude are presented in Figure 4. Figure 4 a) c) e) show an increase in the average values of TWSA and SMA in 2009–2011 for latitudes 0–20°S with a slight standard deviation for these latitudes in the given years. Both sensors picked up the same anomaly in these areas. Time series analyses in this area can be characterized by high convergence. For latitudes 20–40°N, we observe a significant TWSA anomaly that was not captured by the AMSR-E sensors. In the years 2003–2005, we observed a significant standard deviation of anomalies, which indicates a large scatter of observations and substantial variability, which was not captured when determining the average SMA values.

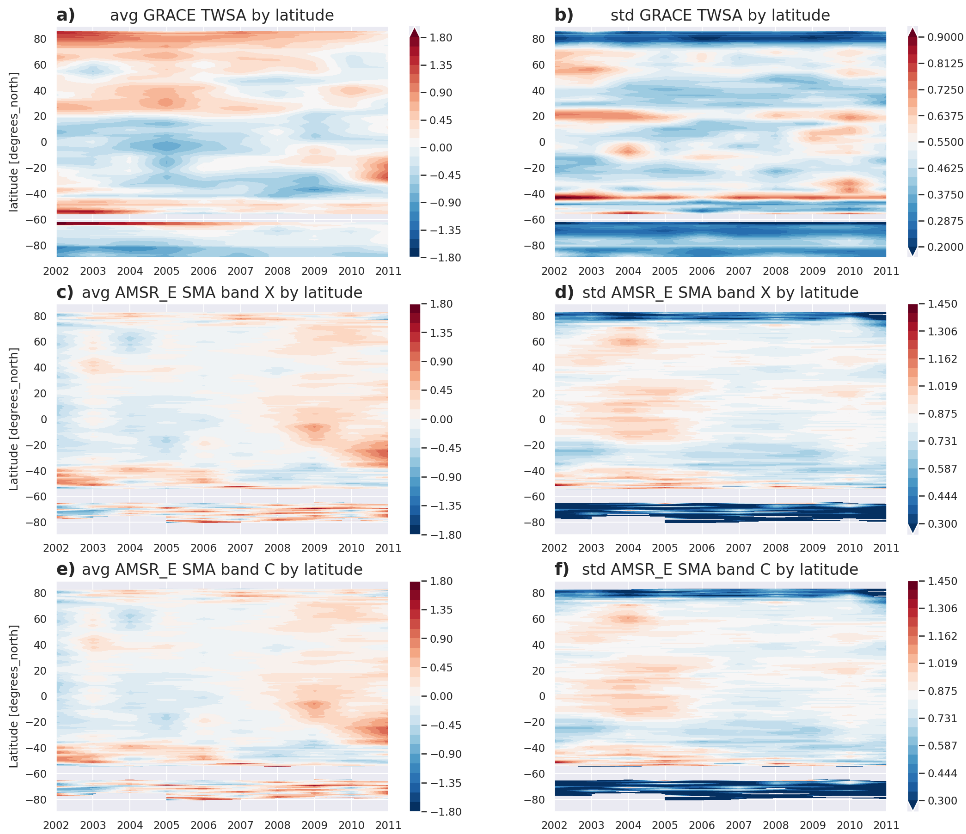

Figure 4. GRACE (a,b) and AMSR-E (c,d,e,f) average anomaly (a,c,e) and standard deviation (b,d,f) grouped by latitude over time

As the data on the water content in the ground shows the cycle of seasonal changes in the groundwater level, the average values were compared separately for each season of the year. The analysis was divided into the C and X bands for the SM observation. After normalizations of ΔTWS, ΔTWS and SM signals were grouped for the winter, spring, summer, and autumn seasons. Where winter months are marked as December, January, February (DJF), spring as March, April, May (MAM), summer as June, July, August (JJA), and autumn as September, October, and November (SON).

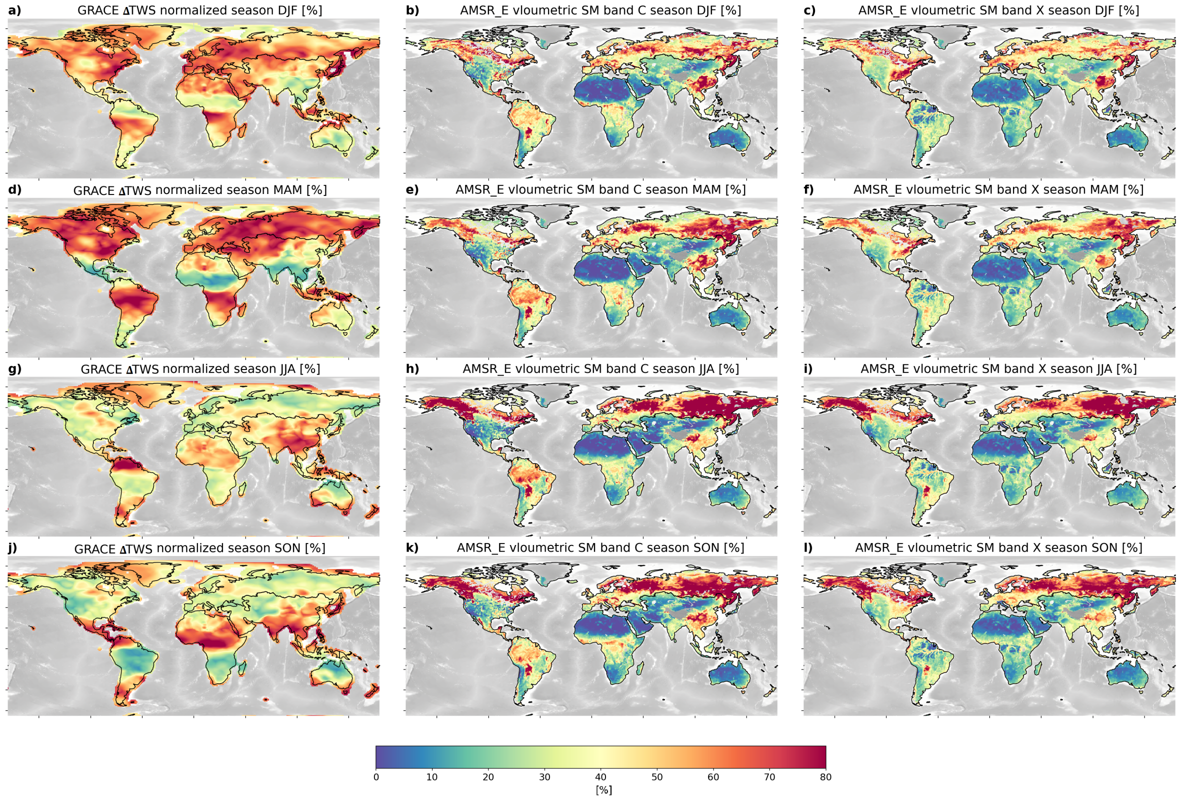

Figure 5. GRACE ΔTWS (a,d,g,j) and AMSR-E band C (b,e,h,k) and band X (c,f,i,l) SM averaged and normalized values grouped by seasons DJF (a,b,c), MAM (g,h,i), JJA (j,k,l) and SON (j,k,l)

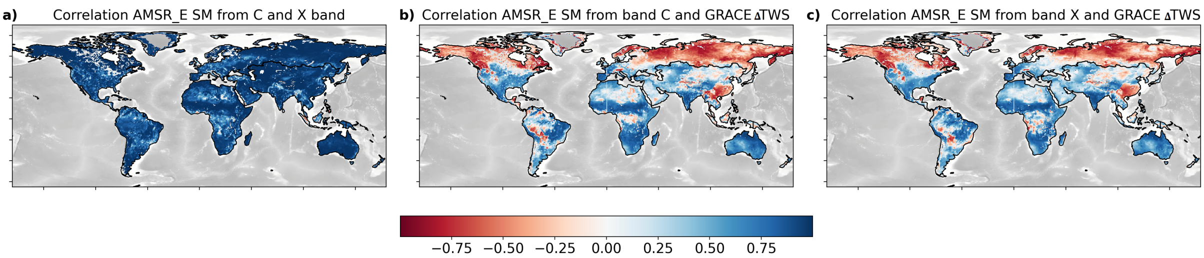

Figure 6. Pearson correlation coefficient between SM from band X and C from AMSR-E (a), ΔTWS from GRACE and SM from band C from AMSR-E (b), ΔTWS from GRACE and SM from band X from AMSR-E (c)

Data from the C- and X-ranges are very similar. However, they are visible in the saturation of the SM parameter. In Figure 5, higher values of VSM in the areas of Amazonia can be noticed for the C- range and the latitude of 60–70 degrees. When comparing the percentages of GRACE and AMSR-E, there are apparent differences. Some of them may be due to data noise in GRACE. Theoretically, all observations from the Sahara area should be close to zero due to the near-zero water content in that area. However, variations in the water content around Lake Chad are observed (Boy et al., 2012), which partially explain this effect. More similarities can be seen between the C-band and the GRACE data, especially in the equatorial regions.

Often long-term microwave SM datasets, such as the Climate Change Initiative (CCI), based on C- and X-band observations, are typically masked over densely vegetated areas due to the soil signal's strong attenuation by the vegetation signal canopy (Dorigo et al., 2011, Liu et al., 2011). It is worth emphasizing here that the X-band penetrates only the surface layer, the C-band a bit deeper, into with highly dense vegetation. Both bands cannot penetrate the soil in some cases (El Hajj et al., 2018). Pearson's correlation coefficient for the tested signals is presented in Figure 6.

Significant values of humidity in the X- and C-bands and low coefficients of correlation with GRACE data observed in the northern regions of the globe, are strongly related to the permafrost region. Data from this area deviates significantly in quality from other observations. No reduced correlations can be seen in forest areas during the comparison of the water content obtained from gravimetric and microwave sensors. The central part of Europe and the eastern regions of China are mainly urbanized areas. There we observe a negative correlation between GRACE and AMSR-E sensors. The anthropogenic factor related to the urbanization of space strongly influences the quality of observation (Ahmed et al., 2014, Chen et al., 2019, Wang et al., 2017). A high rate of urbanization also characterizes the Indian subcontinent. Moreover, over 60% of the area is arable land, which, due to the large number of people living in the region, is necessary to produce the right amount of food. Owing to the large open area and the lack of limitations in oxygen availability in the root zones, we can observe a significant amplitude of the SM signal. Phase compliance contributes to a high correlation in this area despite the progressive urbanization of the area, in particular in the X-band. The cultivated areas worldwide showed highly coherent GRACE and AMSR-E signals for GRACE and AMSR-E observations. The open areas do not have barriers or limitations for rainfall, which allows water to penetrate the root zone. The only exception is the eastern part of Europe, for which the overlapping of urbanization factors and soil constraints on oxygen content, and thus lower soil porosity, slows down water penetration into the soil. This causes a phase shift for the observed signals manifested by the negative correlation coefficient in this area.

EOF method is effective due to its capacity to find spatial correlation in spatiotemporal data. ΔTWS retrieved from the GRACE and SM retrieved from AMSR-E missions are decomposed using the EOF method to extract the signal, mainly describing the river discharge along the main gravity stream. Before determining the EOF, the linear trend was removed from the observations to eliminate the bias. Applying orthogonal decomposition MCA to geophysical datasets permits extracting common dominant patterns between two variables. Regions with the same color are in phase, that means their time series correlate with each other, while regions whose color is different are anticorrelated as shown in Figure 8 and Figure 9.

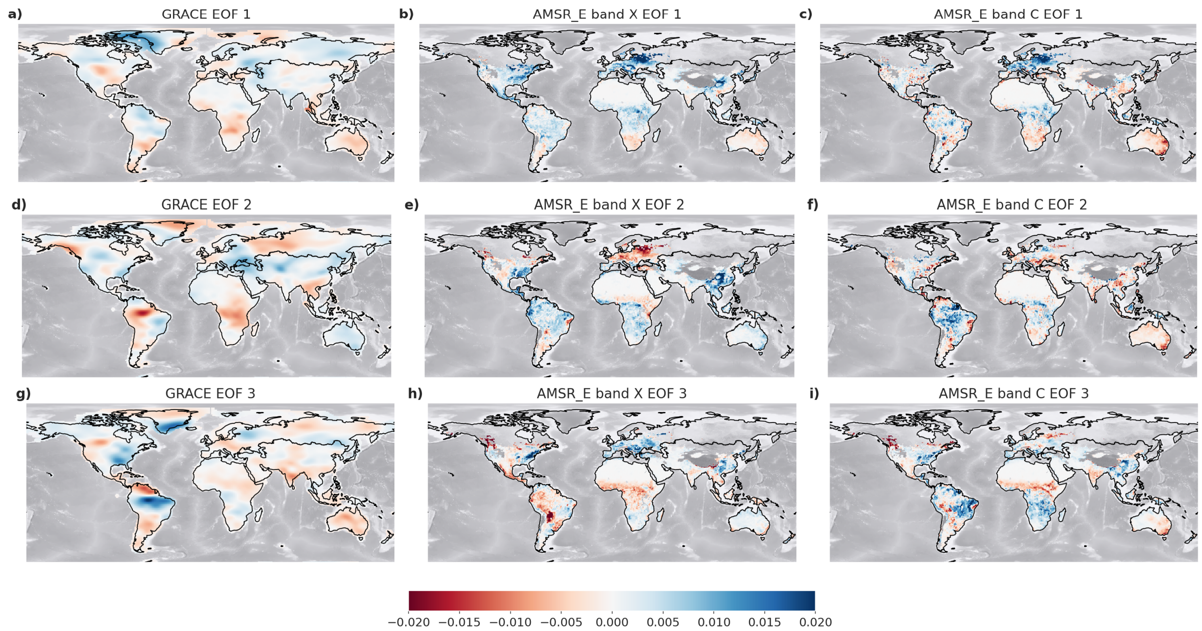

Figure 7. Dominant spatial pattern of water variability presended by decomposition of signal using EOF for ΔTWS from GRACE (a,d,g) and SM from AMSR-E (b,c,e,f,h,j). The first spatial pattern (EOF1) (a,b,c), the second spatial pattern (EOF2) (d,e,f), and the third spatial pattern (EOF3) (g,h,j)

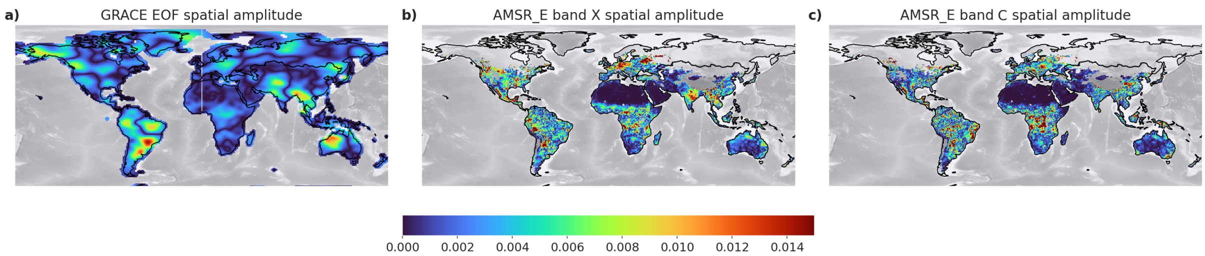

Figure 8. EOF signal amplitude for ΔTWS form GRACE (a), SM from band X from AMSR-E (b), and SM from band C from AMSR-E (c)

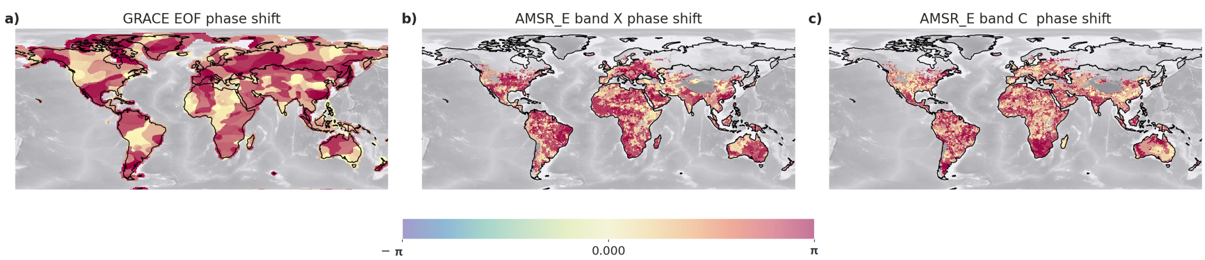

Figure 9. EOF signal phase shift for ΔTWS form GRACE (a), SM from band X from AMSR-E (b), and SM from band C from AMSR-E (c)

4. DISCUSSION

The preservation of the flow of subsurface waters is a significant regional issue, depending on the climate determining the amount of rainwater, the topography, the arrangement of permeable layers, and the presence of river sources. In this part of the article, regional studies were carried out for selected river basins with the most significant area by selecting cases for all continents. Regional analyses appear in earlier articles by Vishwakarma et al. (2021), where time series analysis was carried out for major river basins. In this article, scientists capture significant dips and identify constraints due to too short an observation period using the trend to variability ratio (TVR) metric. This section focuses on the reasons for similarities and differences in gravimetric and microwave signals in selected areas. The observations provided by the GRACE mission are characterized by a significantly lower spatial resolution than microwave observations. The application of grouping to the studied signals within rivers allows for finding patterns resulting from minimizing errors resulting from noise or artifacts of the filtration process. For each continent, a set of rivers with the largest area and different land cover features and different latitudes was selected, thus eliminating bias in the dataset sample. For selected river basins, Pearson's correlation coefficients and cross-correlation, taking into account the phase shift calculated according to formula (2) and presented in Figure 10 and Figure 11, were determined.

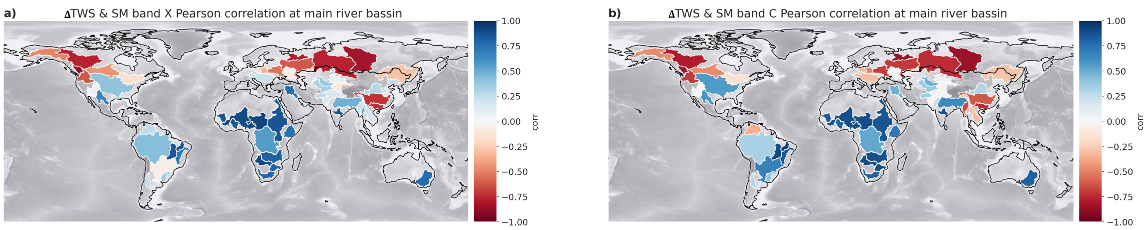

Figure 10. Pearson correlation over selected rivers basin between ΔTWS from GRACE and SM from band X from AMSR-E (a) and ΔTWS from GRACE and SM from band C from AMSR-E (b)

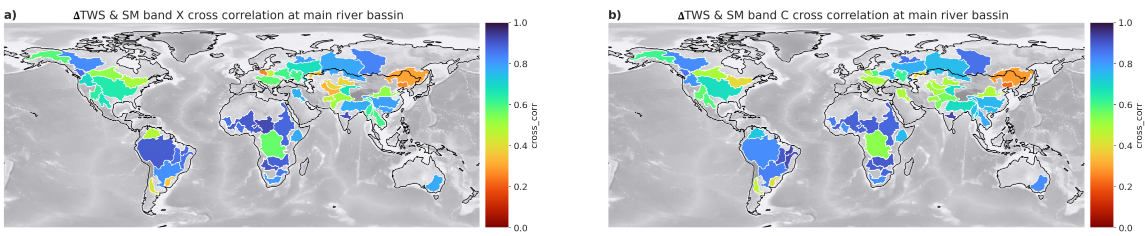

Figure 11. Cross-correlation over selected rivers basin between ΔTWS from GRACE and SM from band X from AMSR-E (a) and ΔTWS from GRACE and SM from band C from AMSR-E (b)

Examples of ΔTWS and SM time series and TWSA and SMA anomalies are shown in Figure 12.

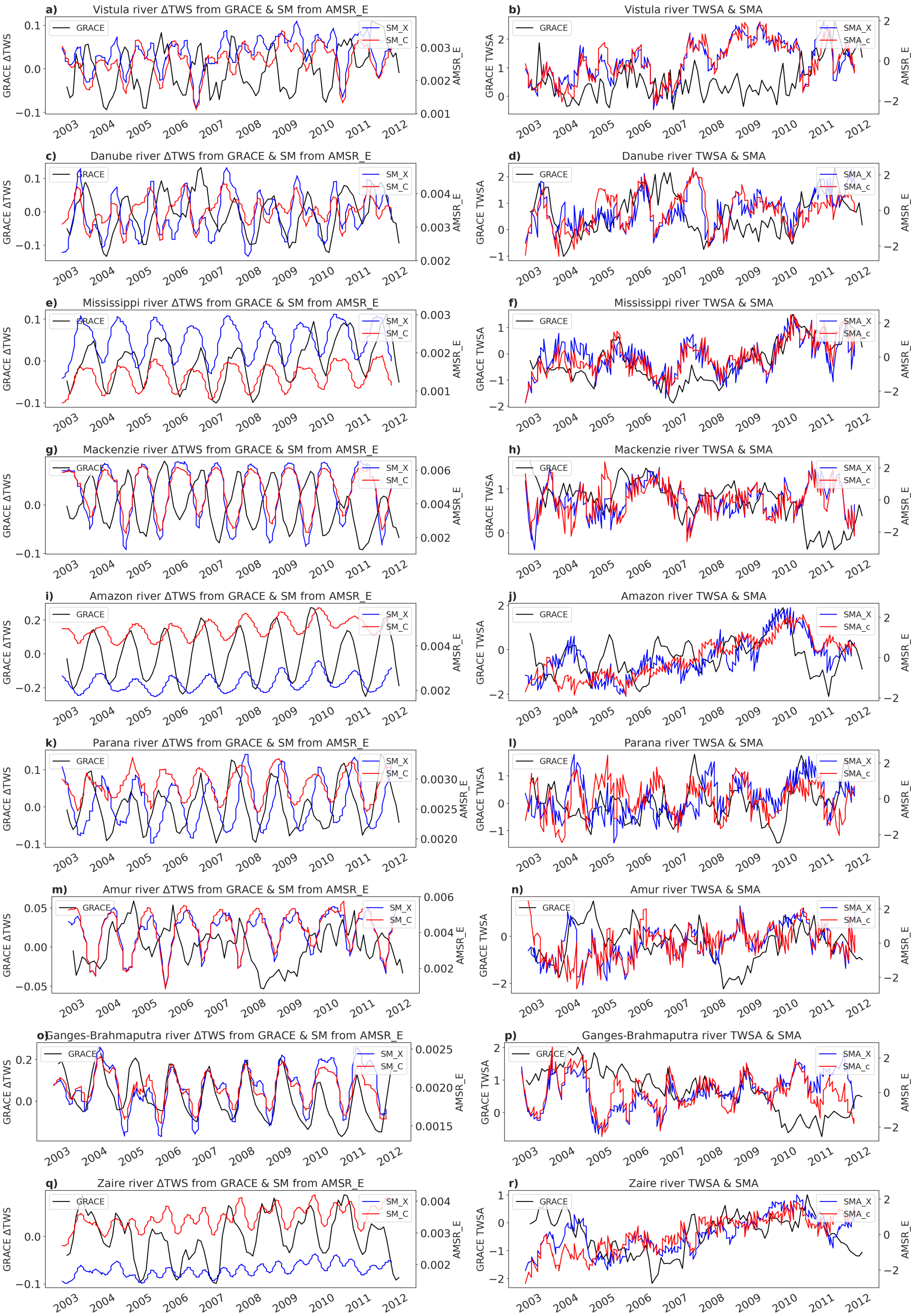
a) Vistula river ΔTWS from GRACE & SM from AMSR_E
b) Vistula river TWSA & SMA
c) Danube river ΔTWS from GRACE & SM from AMSR_E
d) Danube river TWSA & SMA
e) Mississippi river ΔTWS from GRACE & SM from AMSR_E
f) Mississippi river TWSA & SMA
g) Mackenzie river ΔTWS from GRACE & SM from AMSR_E
h) Mackenzie river TWSA & SMA
i) Amazon river ΔTWS from GRACE & SM from AMSR_E
j) Amazon river TWSA & SMA
k) Parana river ΔTWS from GRACE & SM from AMSR_E
l) Parana river TWSA & SMA
m) Amur river ΔTWS from GRACE & SM from AMSR_E
n) Amur river TWSA & SMA
o) Ganges-Brahmaputra river ΔTWS from GRACE & SM from AMSR_E
p) Ganges-Brahmaputra river TWSA & SMA
q) Zaire river ΔTWS from GRACE & SM from AMSR_E
r) Zaire river TWSA & SMA
GRACE ΔTWS
GRACE TWSA
AMSR_E
GRACE
SM_X
SM_C
SMA_X
SMA_c
2003 2004 2005 2006 2007 2008 2009 2010 2011 2012

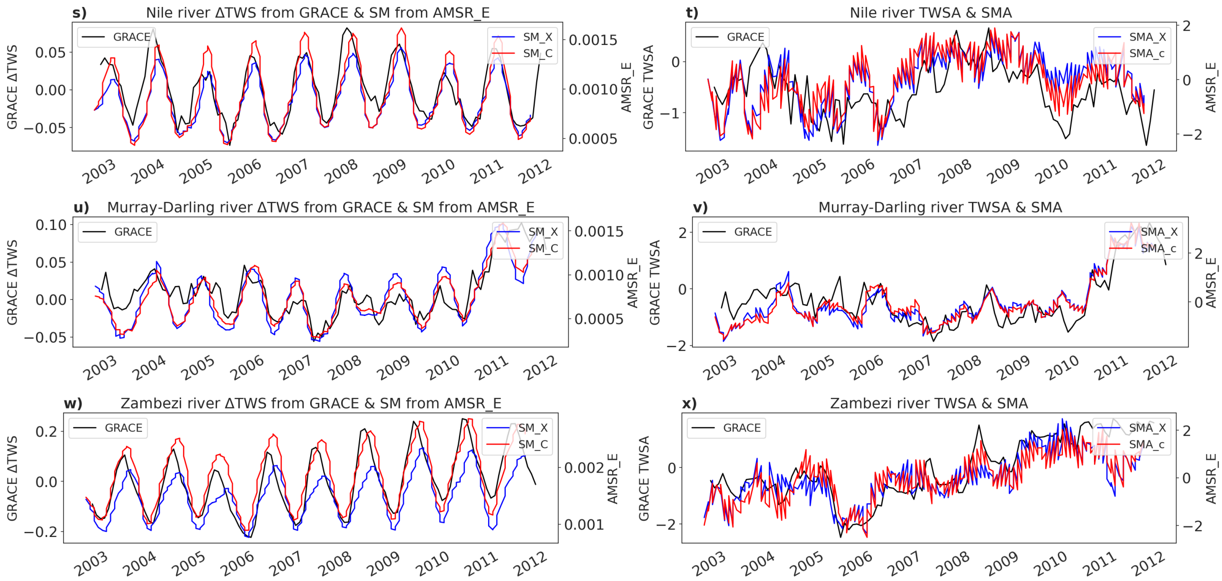

Figure 12. River basin time series containing ΔTWS and SM (a,c,e,g,i,k,m,o,q,s,u,w), TWSA and SMA (b,d,f,h,j,l,n,p,r,t,v,x) for European (a,b,c,d), North America (e,f,g,h), South America (i,j,k,l), Asian (m,n,o,p), African (q,r,s,t,w,x), and Australian (u,v) rivers

4.1. Europe

The analysis shows that the size of the river basin is not directly related to the differences in GRACE and AMSR-E signals. Large European rivers, such as the Danube and the Vistula, show the mutual shift of hydrological signals for gravimetric and microwave remote sensors as can be seen in Figure 12 a), c). There is a more significant variance in the signal for observations from the X- and C-bands than in GRACE observations. Therefore, the determined anomalies are characterized by high noise for these ranges. Similar to the analysis performed in Kuczynska-Siehien et al. (2019), the GRACE and AMSR-E sensors pick up an anomaly related to the 2010 hydrological flood. However, contrary to the cited article, the SM determined from AMSR-E indicates the occurrence of anomalies in the years 2007–2009, which is not recorded in the GLDAS models. The snowfall in these regions during the months of DJF indicates a lower moisture content in the soil, while GRACE sensors capture the mass contained in the snow equivalent. This is explained by the method used to process AMSR-E data. Under frozen surface conditions, the dielectric properties of the water change dramatically. Therefore, the method assigns all pixels where the surface temperature is observed to be at or below 273 K with an appropriate data flag (Holmes et al., 2009).

4.2. Africa

The Nile basin shows a very high agreement between GRACE and AMSR-E signals in both X- and C-bands for the ΔTWS and SM values and their anomalies. The Pearson correlation coefficient between these variables is greater than 0.8 for this region. The lack of soil constraints and little human intervention in the form of agricultural or urban activities contribute to the consistency of observations (Gossel et al., 2004). The percentage of arable land with additional irrigation is less than 5% (Villholth, 2013). In the case of the Nile, a significant factor influencing the changes in ΔTWS is surface runoff. The weather extremes and climatic variances observed over the years using gravimetric observations indicate the high sensitivity of these sensors to extreme phenomena such as droughts (Scanlon et al., 2022, Seka et al., 2022a,b). The GRACE and AMSR-E sensors catch the 2005 and 2010 drought anomalies, shown in Figure 12 t). Similar results were also described by Seka et al. (2022b) using meteorological drought indicators and a water storage deficit index (WSDI) occurring at the source of the Nile in the Turkana, Victoria, and Tanganyika lakes.

The Congo River basin, known as Zaire, is over 60% covered by tropical forests. Crops account for only 10% of the area. The correlation of gravimetric and microwave signals is lower than at the same latitude for the Amazon basin. In this case, data collected by the AMSR-E mission detects two seasonal signal peaks, while GRACE usually has only one, as presented in Figure 12 q), r). The X-band observations for shallow soil layers do not detect a split between longer and shorter rainfall. At the same time, the C-band distinguishes subeasonal changes more like the GRACE observations. Despite the lack of soil constraints, such a large area affected by changes in precipitation caused by the movement of circulation cells poses a challenge for scientists in interpreting ΔTWS and SM observations.

The Zambezi River basin maintained an above-average consistency between GRACE and AMSR-E signals in both X- and C-bands for the ΔTWS and SM values and their anomalies also described in Thomas et al. (2014) and Hassan and Jin (2016). Similar to Thomas et al. (2014), a water deficit was observed in the area Zambezi River basin due to a hydrological drought event in April 2005. For the Zambezi and Zaire river basins, the highest amplitudes of ΔTWS and SM signals on the African continent can be observed. It can therefore be concluded, similarly to the publication of Hassan and Jin (2016), that the ΔTWS in these regions is dominated mainly by precipitation. Despite the relatively poorly urbanized area, the most important anthropogenic factors include that the Zambezi River is used to produce electricity for southern Africa. In the middle stretch of the river, there is a large artificial water reservoir called Kariba. Incremental storage of a large mass of water favors capturing this effect by GRACE sensors with a minor time frequency. Large uncovered agricultural areas and lack of factors contributing to noise in microwave observations contribute to a significant convergence of results with gravimetric sensors.

4.3. North America

The large rivers of North America have different results for the studied similarity between gravimetric and microwave observations. The Mackenzie River basin has its source in Great Slave Lake. Located in the north of Canada in subpolar regions, the source is closely related to the snow equivalent variances visible in the GRACE observations but not included in the X- and C-bands. A similar situation will be seen in the subpolar regions of the Ob River. This result is visible in small correlations and low aggregation of ΔTWS and SM signals and their anomalies.

The Mississippi River basin has the opposite statistics compared to the Mackenzie River described previously. The high agreement of ΔTWS and SM observations, shown by the cross-correlation coefficient > 0.7, is due to the large area of agricultural crops. No limitations for soil conditions, and $<10\%$ afforestation of the area does not retain water in the vegetation and allows free seepage to groundwater. The main components of EOF3 show similar signal strength in terms of area. Observations in the X-range have a slightly more substantial phase shift than observations from the C microwave band. However, the difference is not significant in the context of the examined similarity to gravimetric observations. The high compatibility of TWSA and SMA allows both sensors to quickly monitor and predict natural disasters caused by droughts or floods (Foroumandi et al., 2022).

4.4. South America

The Amazon basin, well described in the literature previously by Chen et al. (2009), Cui et al. (2020, 2022), Eom et al. (2017) and Wu et al. (2022), is exceptionally consistent for GRACE and AMSR-E signals despite being mostly forested. Observations in the X-band captured the 2004 anomaly, which is not visible in the C-band observations. Both bands indicated an anomaly in 2009 resulting from the exceptional flood in this area (Chen et al., 2010b) and droughts in 2010–2012 (Nie et al., 2015). As in the two previously mentioned publications, extreme hydrological phenomena from 2009 to 2012 were captured by the GRACE and AMSR-E sensors in Figure 12 j). A large area and one of the largest amplitudes of water fluctuations resulting from tropical rains occurring at equatorial latitudes cause, despite minor soil limitations, the studied signals to be characterized by considerable convergence.

The La Plata basin region is characterized by a significant anomaly in the GRACE and AMSR-E observations in Figure 4. Extremes occurring in this area require special attention during interpretation (Abelen et al., 2015, Chen et al., 2010a). The low topographic complexity facilitates penetration of the microwave signal. Secondly, a higher value of EOF3 shown in Figure 7 in the X-band AMSR-E indicates the occurrence of phenomena that in the literature can be found as the flood of winter 2009/2010. It was correlated with the occurrence of the El Niño effect and the droughts occurring in 2009. The analysis of the main components indicates that extreme hydrological phenomena have a significant effect both in gravimetric and microwave data. However, due to the differentiation in the La Plata river basin, these phenomena are characterized by a phase shift.

4.5. Asia

The Amur is the tenth longest river in the world, forming the border between the Russian Far East and Northeast China. From the north of the basin, the area covers permafrost and is covered with the boreal forest. The southern part of the area is intensively cultivated and distorted by human activity. As can be seen in Figure 11, the cross-correlation coefficient is at the level of 0.3, which proves the extremely poor compatibility of the ΔTWS and SM signals. This is also confirmed in Figure 12 m), n) presenting the time series for this area. Extreme droughts and wildfires in 2008 described previously in Semenov et al. (2017) are reflected in GRACE observations in this research, represented by an anomaly in this period, which is entirely absent in microwave observations.

The Ganges and Brahmaputra valley is intensively used for agriculture and densely populated area near the Himalayas. The monsoons in this area have become a permanent part of the landscape of the local population. ΔTWS observations in that area were previously described by Felfelani et al. (2017), Forootan et al. (2016) and Papa et al. (2015). Figure 12 o) shows a good agreement between the ΔTWS and SM signals. Cross-correlation over this basin is at a level of 0.75. However, Figure 12 p) shows the discrepancy between TWSA and SMA characterized by the opposite trend in the 2006–2012 period. A similar difference was noted in (Felfelani et al., 2017), described as a significant divergence between the SM natural and GRACE ΔTWS trend lines. As in the case of the Zaire River, the observations provided by the AMSR-E mission capture two annual waves and only one primary wave during GRACE. In this case, the differences between the X- and C-bands are smaller than in the case of the Congo Basin. Strong amplitudes of GRACE and AMSR-E signals, especially in the X-range, presented in Figure 8 a), b) indicate the intensity of SM changes in shallow layers for the largest river delta in the world.

4.6. Australia

The Murray-Darling basin is a large geographic area in the interior of south-eastern Australia with intensive farmland use around Adelaide. The area is characterized by one of the best TWSA and SMA signal correspondences observed in Figure 12 v). The decreasing trend of water content in the soil in this area was described by Heimhuber et al. (2019), Tregoning et al. (2012) and Yang et al. (2014). We see considerable agreement in the detected anomaly in 2010-2011 for gravimetric and microwave sensors. Similar conclusions as in the article by Heimhuber et al. (2019) can be obtained regarding the interpretation of the results from the period 2010–2012. La Nina Floods can be observed in higher TWSA and SMA in Figure 12 v). Unlike previous works, ASMR-E sensors did not show decreasing trend related to the 2000–2009 Millennium Drought. This is partly explained by the aggregation of data over a large river basin area and the different intensification of phenomena in the northern and southern parts of the river basin. Observations in the C-band compared to GRACE are similar in phase. Figure 9 shows a more significant shift in the observations of the X-band for its main components, which explains the shallow penetration into the soil layers for this band. However, the lack of significant global constraints, large open spaces, and small built-up areas create favorable conditions for the GRACE and AMSR-E satellites to detect the same groundwater characteristics and variances. The high Pearson correlation coefficient at the level of 0.8 and the cross-correlation of about 0.7 are visible in Figure 10 and Figure 11.

5. CONCLUSIONS

This article discusses the conditions under which the ΔTWS observations provided by the gravimetric GRACE mission are characterized by a greater or lesser signal convergence with the observations provided by the passive multiwavelength microwave sensors of the AMSR-E mission. The interplay of ΔTWS and SM can provide a better and high-resolution understanding of the Earth's processes related to the water cycle. The complexity of land uses processes and conditions impacts the detection and mapping of natural hazards, such as droughts or floods, observed on a global or regional scale. Understanding the limitations affecting the speed of detection of changes and consistency in the observations provided using various methods and sensors has a tangible impact on the quality of the solutions provided for the prediction of geo-hazards. The main conclusions and observations from the conducted study worth emphasizing are the mutual relationship between the use of cultivated and forested areas in the ΔTWS and SM compliance analyses. Naturally forested areas and large open spaces used for agriculture support the compatibility between GRACE and AMSR-E observations. The discussion showed a high correlation for these areas, at the same time pointing to the importance of good oxygen conditions for root zones in the soil. Existing soil constraints such as permafrost significantly eliminate the usefulness of X- and C-range microwave observations. For this reason, analyses carried out in subpolar regions using gravimetric sensors have a significant advantage. The referenced examples in the subsection for Europe indicate differences between GRACE and AMSR-E in signals leading to the conclusion of unfavorable conditions resulting from soil constraints and significant urbanization of the area. Moreover, the study opens the question of spatial data leakage caused by filtering low-resolution GRACE data. Regions with high signal variance averaged over the area of the entire river basin may cause the loss of a part of the geophysical signal, which was observed and described for the example of the Zaire River. The use of mathematical methods and a combination of signals with different spatial and temporal resolutions, for areas with appropriate conditions and no soil and urban restrictions, will be the next direction of the research.

Acknowledgments.

Data availability:

Data from the GRACE mission was collected from https://podaac-tools.jpl.nasa.gov/ distributed by the Center for Space Research (CSR). AMSR-E dataset was downloaded as daily files from https://disc.gsfc.nasa.gov/. To analyze land cover conditions The Harmonized World Soil Database was used from https://www.fao.org/soils-portal/data-hub/.

Declaration of Competing Interest:

The authors declare that they have no known competing financial interests or personal relationships that could have appeared to influence the work reported in this article.

REFERENCES

Abelen, S. and Seitz, F. (2013). Relating satellite gravimetry data to global soil moisture products via data harmonization and correlation analysis. *Remote Sensing of Environment*, 136:89–98.

Abelen, S., Seitz, F., Abarca-del Rio, R., and Güntner, A. (2015). Droughts and floods in the la plata basin in soil moisture data and grace. *Remote Sensing*, 7(6):7324–7349.

Abelen, S., Seitz, F., Schmidt, M., and Güntner, A. (2011). Analysis of regional variations in soil moisture by means of remote sensing, satellite gravimetry and hydrological modelling. *GRACE, Remote Sensing and Ground-Based Methods in Multi-Scale Hydrology, IAHS Red Book Series*, (343):9–15.

Ahmed, M., Sultan, M., Wahr, J., and Yan, E. (2014). The use of grace data to monitor natural and anthropogenic induced variations in water availability across africa. *Earth-Science Reviews*, 136:289–300.

Babaeian, E., Sadeghi, M., Jones, S. B., Montzka, C., Vereecken, H., and Tuller, M. (2019). Ground, proximal, and satellite remote sensing of soil moisture. *Reviews of Geophysics*, 57(2):530–616.

Bartalis, Z., Wagner, W., Naeimi, V., Hasenauer, S., Scipal, K., Bonekamp, H., Figa, J., and Anderson, C. (2007). Initial soil moisture retrievals from the metop-a advanced scatterometer (ascat). *Geophysical Research Letters*, 34(20).

Betts, A. K., Ball, J. H., Beljaars, A., Miller, M., and Viterbo, P. (1994). Coupling between land-surface boundary-layer parameterizations and rainfall on local and regional scales: Lessons from the wet summer of 1993. In *Fifth Symp. on Global Change Studies*, pages 174–181.

Boy, J.-P., Hinderer, J., and de Linage, C. (2012). Retrieval of large-scale hydrological signals in africa from grace time-variable gravity fields. *Pure and applied Geophysics*, 169(8):1373–1390.

Chen, F., Crow, W. T., Bindlish, R., Colliander, A., Burgin, M. S., Asanuma, J., and Aida, K. (2018). Global-scale evaluation of smap, smos and ascat soil moisture products using triple collocation. *Remote Sensing of Environment*, 214:1–13.

Chen, H., Zhang, W., Nie, N., and Guo, Y. (2019). Long-term groundwater storage variations estimated in the songhua river basin by using grace products, land surface models, and in-situ observations. *Science of the Total Environment*, 649:372–387.

Chen, J., Wilson, C., Tapley, B., Longuevergne, L., Yang, Z., and Scanlon, B. (2010a). Recent la plata basin drought conditions observed by satellite gravimetry. *Journal of Geophysical Research: Atmospheres*, 115(D22).

Chen, J., Wilson, C., Tapley, B., Yang, Z., and Niu, G.-Y. (2009). 2005 drought event in the amazon river basin as measured by grace and estimated by climate models. *Journal of Geophysical Research: Solid Earth*, 114(B5).

Chen, J. L., Wilson, C. R., and Tapley, B. D. (2010b). The 2009 exceptional amazon flood and interannual terrestrial water storage change observed by grace. *Water Resources Research*, 46(12).

Chen, J. L., Wilson, C. R., Tapley, B. D., and Grand, S. (2007). Grace detects coseismic and postseismic deformation from the sumatra-andaman earthquake. *Geophysical Research Letters*, 34(13).

Chen, X.-z., Chen, S.-s., Zhong, R.-f., Su, Y.-x., Liao, J.-s., Li, D., Han, L.-s., Li, Y., and Li, X. (2012). A semi-empirical inversion model for assessing surface soil moisture using amsr-e brightness temperatures. *Journal of hydrology*, 456:1–11.

Chen, Y., Yang, K., Qin, J., Zhao, L., Tang, W., and Han, M. (2013). Evaluation of amsr-e retrievals and gldas simulations against observations of a soil moisture network on the central tibetan plateau. *Journal of Geophysical Research: Atmospheres*, 118(10):4466–4475.

Cheng, M. and Tapley, B. D. (2004). Variations in the earth's oblateness during the past 28 years. *Journal of Geophysical Research: Solid Earth*, 109(B9).

Crow, W. T., Berg, A. A., Cosh, M. H., Loew, A., Mohanty, B. P., Panciera, R., de Rosnay, P., Ryu, D., and Walker, J. P. (2012). Upscaling sparse ground-based soil moisture observations for the validation of coarse-resolution satellite soil moisture products. *Reviews of Geophysics*, 50(2).

Crow, W. T., Han, E., Ryu, D., Hain, C. R., and Anderson, M. C. (2017). Estimating annual water storage variations in medium-scale (2000–10 000 km 2) basins using microwave-based soil moisture retrievals. *Hydrology and Earth System Sciences*, 21(3):1849–1862.

Crow, W. T., Lei, F., Hain, C., Anderson, M. C., Scott, R. L., Billesbach, D., and Arkebauer, T. (2015). Robust estimates of soil moisture and latent heat flux coupling strength obtained from triple collocation. *Geophysical Research Letters*, 42(20):8415–8423.

Cui, L., Song, Z., Luo, Z., Zhong, B., Wang, X., and Zou, Z. (2020). Comparison of terrestrial water storage changes derived from grace/grace-fo and swarm: A case study in the amazon river basin. *Water*, 12(11):3128.

Cui, L., Yin, M., Huang, Z., Yao, C., Wang, X., and Lin, X. (2022). The drought events over the amazon river basin from 2003 to 2020 detected by grace/grace-fo and swarm satellites. *Remote Sensing*, 14(12):2887.

Dahle, C., Flechtner, F., Gruber, C., König, D., König, R., Michalak, G., and Neumayer, K.-H. (2013). Gfz grace level-2 processing standards document for level-2 product release 0005: revised edition, january 2013.

De Jeu, R. A., Wagner, W., Holmes, T., Dolman, A., Van De Giesen, N., and Friesen, J. (2008). Global soil moisture patterns observed by space borne microwave radiometers and scatterometers. *Surveys in Geophysics*, 29(4):399–420.

Dorigo, W., Wagner, W., Hohensinn, R., Hahn, S., Paulik, C., Xaver, A., Gruber, A., Drusch, M., Mecklenburg, S., van Oevelen, P., et al. (2011). The international soil moisture network: a data hosting facility for global in situ soil moisture measurements. *Hydrology and Earth System Sciences*, 15(5):1675–1698.

Draper, C. S., Walker, J. P., Steinle, P. J., De Jeu, R. A., and Holmes, T. R. (2009). An evaluation of amsr–e derived soil moisture over australia. *Remote Sensing of Environment*, 113(4):703–710.

Du, J., Kimball, J., Velicogna, I., Zhao, M., Jones, L., Watts, J., and Kim, Y. (2019). Multicomponent satellite assessment of drought severity in the contiguous united states from 2002 to 2017 using amsr-e and amsr2. *Water Resources Research*, 55(7):5394–5412.

El Hajj, M., Baghdadi, N., Bazzi, H., and Zribi, M. (2018). Penetration analysis of sar signals in the c and l bands for wheat, maize, and grasslands. *Remote Sensing*, 11(1):31.

Engman, E. T. (1992). Soil moisture needs in earth sciences. In *In: IGARSS'92; Proceedings of the 12th Annual International Geoscience and Remote Sensing Symposium, Houston, TX, May 26-29, 1992. Vol. 1 (A93-47551 20-43)*. Institute of Electrical and Electronics Engineers, Inc.

Entekhabi, D., Nakamura, J., and Njoku, E. (1994). Retrieval of soil moisture profile by combined remote sensing and modeling. *Passive Microwave Remote Sensing of Land-Atmosphere Interactions: [ESA/NASA International Workshop, Held at Saint Lary (France) from January 11–15, 1993]*.

Eom, J., Seo, K.-W., and Ryu, D. (2017). Estimation of amazon river discharge based on eof analysis of grace gravity data. *Remote Sensing of Environment*, 191:55–66.

Famiglietti, J. S., Ryu, D., Berg, A. A., Rodell, M., and Jackson, T. J. (2008). Field observations of soil moisture variability across scales. *Water Resources Research*, 44(1).

Fast, J. D. and McCorcle, M. D. (1991). The effect of heterogeneous soil moisture on a summer baroclinic circulation in the central united states. *Monthly weather review*, 119(9):2140–2167.

Felfelani, F., Wada, Y., Longuevergne, L., and Pokhrel, Y. N. (2017). Natural and human-induced terrestrial water storage change: A global analysis using hydrological models and grace. *Journal of Hydrology*, 553:105–118.

Fischer, G., Nachtergaele, F., Prieler, S., Van Velthuizen, H., Verelst, L., and Wiberg, D. (2008). Global agro-ecological zones assessment for agriculture (gaez 2008). *IIASA, Laxenburg, Austria and FAO, Rome, Italy*, 10.

Flechtner, F., Neumayer, K.-H., Dahle, C., Dobslaw, H., Fagiolini, E., Raimondo, J.-C., and Güntner, A. (2016). What can be expected from the grace-fo laser ranging interferometer for earth science applications? In *Remote sensing and water resources*, pages 263–280. Springer.

Forootan, E., Schumacher, M., Awange, J. L., and Müller Schmied, H. (2016). Exploring the influence of precipitation extremes and human water use on total water storage (tws) changes in the g anges-b rahmaputra-m eghna river basin. *Water Resources Research*, 52(3):2240–2258.

Foroumandi, E., Nourani, V., Huang, J. J., and Moradkhani, H. (2022). Drought monitoring by downscaling grace-derived terrestrial water storage anomalies: a deep learning approach. *Journal of Hydrology*, page 128838.

Frappart, F. and Ramillien, G. (2018). Monitoring groundwater storage changes using the gravity recovery and climate experiment (grace) satellite mission: A review. *Remote Sensing*, 10(6):829.

Fu, T.-c. (2011). A review on time series data mining. *Engineering Applications of Artificial Intelligence*, 24(1):164–181.

Gossel, W., Ebraheem, A., and Wycisk, P. (2004). A very large scale gis-based groundwater flow model for the nubian sandstone aquifer in eastern sahara (egypt, northern sudan and eastern libya). *Hydrogeology Journal*, 12(6):698–713.

Gruber, A., Dorigo, W. A., Crow, W., and Wagner, W. (2017). Triple collocation-based merging of satellite soil moisture retrievals. *IEEE Transactions on Geoscience and Remote Sensing*, 55(12):6780–6792.

Haining, R. P., Kerry, R., and Oliver, M. A. (2010). Geography, spatial data analysis, and geostatistics: An overview. *Geographical Analysis*, 42(1):7–31.

Hasan, E. and Tarhule, A. (2021). Comparison of decadal water storage trends from common grace releases (rl05, rl06) using spatial diagnostics and a modified triple collocation approach. *Journal of Hydrology X*, 13:100108.

Hassan, A. and Jin, S. (2016). Water storage changes and balances in africa observed by grace and hydrologic models. *Geodesy and Geodynamics*, 7(1):39–49.

Heimhuber, V., Tulbure, M. G., Broich, M., Xie, Z., and Hurriyet, M. (2019). The role of grace total water storage anomalies, streamflow and rainfall in stream salinity trends across australia's murray-darling basin during and post the millennium drought. *International Journal of Applied Earth Observation and Geoinformation*, 83:101927.

Holmes, T., De Jeu, R., Owe, M., and Dolman, A. (2009). Land surface temperature from ka band (37 ghz) passive microwave observations. *Journal of Geophysical Research: Atmospheres*, 114(D4).

Jackson, T., Hawley, M., and O'neill, P. (1987). Preplanting soil moisture using passive microwave sensors 1. *JAWRA Journal of the American Water Resources Association*, 23(1):11–19.

Jackson, T. J., Cosh, M. H., Bindlish, R., Starks, P. J., Bosch, D. D., Seyfried, M., Goodrich, D. C., Moran, M. S., and Du, J. (2010). Validation of advanced microwave scanning radiometer soil moisture products. *IEEE Transactions on Geoscience and Remote Sensing*, 48(12):4256–4272.

Kerr, Y. H., Al-Yaari, A., Rodriguez-Fernandez, N., Parrens, M., Molero, B., Leroux, D., Bircher, S., Mahmoodi, A., Mialon, A., Richaume, P., et al. (2016). Overview of smos performance in terms of global soil moisture monitoring after six years in operation. *Remote Sensing of Environment*, 180:40–63.

Khaki, M., Schumacher, M., Forootan, E., Kuhn, M., Awange, J. L., and van Dijk, A. I. (2017). Accounting for spatial correlation errors in the assimilation of grace into hydrological models through localization. *Advances in Water Resources*, 108:99–112.

Koike, T., Nakamura, Y., Kaihotsu, I., Davaa, G., Matsuura, N., Tamagawa, K., and Fujii, H. (2004). Development of an advanced microwave scanning radiometer (amsr-e) algorithm for soil moisture and vegetation water content. *Proceedings of Hydraulic Engineering*, 48:217–222.

Kuczynska-Siehien, J., Piretzidis, D., Sideris, M. G., Olszak, T., and Szabó, V. (2019). Monitoring of extreme land hydrology events in central poland using grace, land surface models and absolute gravity data. *Journal of Applied Geodesy*, 13(3):229–243.

Kumar, S. V., Dirmeyer, P. A., Peters-Lidard, C. D., Bindlish, R., and Bolten, J. (2018). Information theoretic evaluation of satellite soil moisture retrievals. *Remote sensing of environment*, 204:392–400.

Landerer, F. W. and Swenson, S. (2012). Accuracy of scaled grace terrestrial water storage estimates. *Water resources research*, 48(4).

Lei, J., Matsuo, T., Dou, X., Sutton, E., and Luan, X. (2012). Annual and semiannual variations of thermospheric density: Eof analysis of champ and grace data. *Journal of Geophysical Research: Space Physics*, 117(A1).

Liu, Y., Dorigo, W. A., Parinussa, R., de Jeu, R. A., Wagner, W., McCabe, M. F., Evans, J., and

Van Dijk, A. (2012). Trend-preserving blending of passive and active microwave soil moisture retrievals. *Remote Sensing of Environment*, 123:280–297.

Liu, Y. Y., Parinussa, R., Dorigo, W. A., De Jeu, R. A., Wagner, W., Van Dijk, A., McCabe, M. F., and Evans, J. (2011). Developing an improved soil moisture dataset by blending passive and active microwave satellite-based retrievals. *Hydrology and Earth System Sciences*, 15(2):425–436.

Longuevergne, L., Scanlon, B. R., and Wilson, C. R. (2010). Grace hydrological estimates for small basins: Evaluating processing approaches on the high plains aquifer, usa. *Water Resources Research*, 46(11).

Martínez-Fernández, J. and Ceballos, A. (2005). Mean soil moisture estimation using temporal stability analysis. *Journal of Hydrology*, 312(1-4):28–38.

Navarra, A. and Simoncini, V. (2010). *A guide to empirical orthogonal functions for climate data analysis*. Springer Science & Business Media.

Nie, N., Zhang, W., Guo, H., and Ishwaran, N. (2015). 2010–2012 drought and flood events in the amazon basin inferred by grace satellite observations. *Journal of Applied Remote Sensing*, 9(1):096023.

Njoku, E. G., Ashcroft, P., Chan, T. K., and Li, L. (2005). Global survey and statistics of radio-frequency interference in amsr-e land observations. *IEEE Transactions on Geoscience and Remote Sensing*, 43(5):938–947.

Njoku, E. G. and Entekhabi, D. (1996). Passive microwave remote sensing of soil moisture. *Journal of hydrology*, 184(1-2):101–129.

Njoku, E. G., Jackson, T. J., Lakshmi, V., Chan, T. K., and Nghiem, S. V. (2003). Soil moisture retrieval from amsr-e. *IEEE transactions on Geoscience and remote sensing*, 41(2):215–229.

Owe, M., de Jeu, R., and Walker, J. (2001). A methodology for surface soil moisture and vegetation optical depth retrieval using the microwave polarization difference index. *IEEE Transactions on Geoscience and Remote Sensing*, 39(8):1643–1654.

Papa, F., Frappart, F., Malbeteau, Y., Shamsudduha, M., Vuruputur, V., Sekhar, M., Ramillien, G., Prigent, C., Aires, F., Pandey, R. K., et al. (2015). Satellite-derived surface and sub-surface water storage in the ganges–brahmaputra river basin. *Journal of Hydrology: Regional Studies*, 4:15–35.

Peltier, W., Argus, D. F., and Drummond, R. (2018). Comment on "an assessment of the ice-6g_c (vm5a) glacial isostatic adjustment model" by purcell et al. *Journal of Geophysical Research: Solid Earth*, 123(2):2019–2028.

Petropoulos, G. P., Ireland, G., Srivastava, P. K., and Ioannou-Katidis, P. (2014). An appraisal of the accuracy of operational soil moisture estimates from smos miras using validated in situ observations acquired in a mediterranean environment. *International Journal of Remote Sensing*, 35(13):5239–5250.

Rieger, N., Corral, Á., Olmedo, E., and Turiel, A. (2021). Lagged teleconnections of climate variables identified via complex rotated maximum covariance analysis. *Journal of Climate*, 34(24):9861–9878.

Ries, J., Bettadpur, S., Eanes, R., Kang, Z., Ko, U., McCullough, C., Nagel, P., Pie, N., Poole, S., Richter, T., et al. (2016). The combined gravity model ggm05c. *GFZ Data Services*.

Robinson, D. A., Campbell, C. S., Hopmans, J. W., Hornbuckle, B. K., Jones, S. B., Knight, R., Ogden, F., Selker, J., and Wendroth, O. (2008). Soil moisture measurement for ecological and hydrological watershed-scale observatories: A review. *Vadose Zone Journal*, 7(1):358–389.

Rodell, M., Houser, P., Jambor, U., Gottschalck, J., Mitchell, K., Meng, C.-J., Arsenault, K., Cosgrove, B., Radakovich, J., Bosilovich, M., et al. (2004). The global land data assimilation system. *Bulletin of the American Meteorological society*, 85(3):381–394.

Sadeghi, M., Gao, L., Ebtehaj, A., Wigneron, J.-P., Crow, W. T., Reager, J. T., and Warrick, A. W. (2020). Retrieving global surface soil moisture from grace satellite gravity data. *Journal of Hydrology*, 584:124717.

Saha, S. (1995). Assessment of regional soil moisture conditions by coupling satellite sensor data with a soil-plant system heat and moisture balance model. *Remote Sensing*, 16(5):973–980.

Scanlon, B. R., Rateb, A., Anyamba, A., Kebede, S., MacDonald, A. M., Shamsudduha, M., Small, J., Sun, A., Taylor, R. G., and Xie, H. (2022). Linkages between grace water storage, hydrologic extremes, and climate teleconnections in major african aquifers. *Environmental Research Letters*, 17(1):014046.

Schrama, E. J., Wouters, B., and Lavallée, D. A. (2007). Signal and noise in gravity recovery and climate experiment (grace) observed surface mass variations. *Journal of Geophysical Research: Solid Earth*, 112(B8).

Seka, A. M., Zhang, J., Prodhan, F. A., Ayele, G. T., Finsa, M. M., Sharma, T. P. P., and Melesse, A. M. (2022a). Hydrological drought impacts on water storage variations: a focus on the role of vegetation changes in the east africa region. a systematic review. *Environmental Science and Pollution Research*, pages 1–20.

Seka, A. M., Zhang, J., Zhang, D., Ayele, E. G., Han, J., Prodhan, F. A., Zhang, G., and Liu, Q. (2022b). Hydrological drought evaluation using grace satellite-based drought index over the lake basins, east africa. *Science of The Total Environment*, 852:158425.

Semenov, E., Sokolikhina, N., and Tatarinovich, E. (2017). Monsoon circulation over the amur river basin during catastrophic flood and extreme drought in summer. *Russian Meteorology and Hydrology*, 42(3):141–149.

Seo, K.-W., Ryu, D., Kim, B.-M., Waliser, D. E., Tian, B., and Eom, J. (2010). Grace and amsr-e-based estimates of winter season solid precipitation accumulation in the arctic drainage region. *Journal of Geophysical Research: Atmospheres*, 115(D20).

Sprott, J. C. and Sprott, J. C. (2003). *Chaos and time-series analysis*, volume 69. Oxford university press Oxford.

Sun, Y., Riva, R., and Ditmar, P. (2016). Optimizing estimates of annual variations and trends in geocenter motion and j2 from a combination of grace data and geophysical models. *Journal of Geophysical Research: Solid Earth*, 121(11):8352–8370.

Swenson, S., Chambers, D., and Wahr, J. (2008a). Estimating geocenter variations from a combination of grace and ocean model output. *Journal of Geophysical Research: Solid Earth*, 113(B8).

Swenson, S., Famiglietti, J., Basara, J., and Wahr, J. (2008b). Estimating profile soil moisture and groundwater variations using grace and oklahoma mesonet soil moisture data. *Water Resources Research*, 44(1).

Swenson, S. and Wahr, J. (2002). Methods for inferring regional surface-mass anomalies from gravity recovery and climate experiment (grace) measurements of time-variable gravity. *Journal* *of Geophysical Research: Solid Earth*, 107(B9):ETG–3.

Swenson, S. and Wahr, J. (2006). Post-processing removal of correlated errors in grace data. *Geophysical research letters*, 33(8).

Tangdamrongsub, N., Dong, J., and Shellito, P. (2022). Assessing performances of multivariate data assimilation algorithms with smos, smap, and grace observations for improved soil moisture and groundwater analyses. *Water*, 14(4):621.

Tapley, B. D., Bettadpur, S., Ries, J. C., Thompson, P. F., and Watkins, M. M. (2004a). Grace measurements of mass variability in the earth system. *science*, 305(5683):503–505.

Tapley, B. D., Bettadpur, S., Watkins, M., and Reigber, C. (2004b). The gravity recovery and climate experiment: Mission overview and early results. *Geophysical research letters*, 31(9).

Thomas, A. C., Reager, J. T., Famiglietti, J. S., and Rodell, M. (2014). A grace-based water storage deficit approach for hydrological drought characterization. *Geophysical Research Letters*, 41(5):1537–1545.

Tian, S., Tregoning, P., Renzullo, L. J., van Dijk, A. I., Walker, J. P., Pauwels, V. R., and Allgeyer, S. (2017). Improved water balance component estimates through joint assimilation of grace water storage and smos soil moisture retrievals. *Water Resources Research*, 53(3):1820–1840.

Topp, G. C., Davis, J., and Annan, A. P. (1980). Electromagnetic determination of soil water content: Measurements in coaxial transmission lines. *Water resources research*, 16(3):574–582.

Tregoning, P., McClusky, S., Van Dijk, A., Crosbie, R., and Peña-Arancibia, J. (2012). Assessment of grace satellites for groundwater estimation in australia. *National Water Commission, Canberra*, 82.

Ulaby, F. T. (1982). Microwave remote sensing active and passive. *Rader remote sensing and surface scattering and emission theory*, pages 848–902.

van der Vliet, M., van der Schalie, R., Rodriguez-Fernandez, N., Colliander, A., de Jeu, R., Preimesberger, W., Scanlon, T., and Dorigo, W. (2020). Reconciling flagging strategies for multi-sensor satellite soil moisture climate data records. *Remote Sensing*, 12(20):3439.

Vereecken, H., Huisman, J., Pachepsky, Y., Montzka, C., Van Der Kruk, J., Bogena, H., Weihermüller, L., Herbst, M., Martinez, G., and Vanderborght, J. (2014). On the spatio-temporal dynamics of soil moisture at the field scale. *Journal of Hydrology*, 516:76–96.

Villholth, K. G. (2013). Groundwater irrigation for smallholders in sub-saharan africa–a synthesis of current knowledge to guide sustainable outcomes. *Water International*, 38(4):369–391.

Vinnikov, K. Y., Robock, A., Qiu, S., Entin, J. K., Owe, M., Choudhury, B. J., Hollinger, S. E., and Njoku, E. G. (1999). Satellite remote sensing of soil moisture in illinois, united states. *Journal of Geophysical Research: Atmospheres*, 104(D4):4145–4168.

Vishwakarma, B. D., Bates, P., Sneeuw, N., Westaway, R. M., and Bamber, J. L. (2021). Re-assessing global water storage trends from grace time series. *Environmental Research Letters*, 16(3):034005.

Wagner, W., Hahn, S., Kidd, R., Melzer, T., Bartalis, Z., Hasenauer, S., Figa, J., De Rosnay, P., Jann, A., Schneider, S., et al. (2013). The ascat soil moisture product: A review of its. *Meteorologische Zeitschrift*, 22(1):1–29.

Wahr, J., Molenaar, M., and Bryan, F. (1998). Time variability of the earth's gravity field: Hydrological and oceanic effects and their possible detection using grace. *Journal of Geophysical Research: Solid Earth*, 103(B12):30205–30229.

Wang, J. and Forman, B. (2020). Improved terrestrial snow mass via multi-sensor assimilation of synthetic grace terrestrial water storage retrievals and synthetic amsr-e brightness temperature spectral differences. Technical report, Copernicus Meetings.

Wang, J., Forman, B. A., Girotto, M., and Reichle, R. H. (2021). Estimating terrestrial snow mass via multi-sensor assimilation of synthetic amsr-e brightness temperature spectral differences and synthetic grace terrestrial water storage retrievals. *Water Resources Research*, 57(9):e2021WR029880.

Wang, L., Chen, C., Du, J., and Wang, T. (2017). Detecting seasonal and long-term vertical displacement in the north china plain using grace and gps. *Hydrology and Earth System Sciences*, 21(6):2905–2922.

Wang, R., Huston, S., Li, Y., Ma, H., Peng, Y., and Ding, L. (2018). Temporal stability of groundwater depth in the contemporary yellow river delta, eastern china. *Sustainability*, 10(7):2224.

Wouters, B. and Schrama, E. J. (2007). Improved accuracy of grace gravity solutions through empirical orthogonal function filtering of spherical harmonics. *Geophysical Research Letters*, 34(23).

Wu, W.-Y., Yang, Z.-L., Zhao, L., and Lin, P. (2022). The impact of multi-sensor land data assimilation on river discharge estimation. *Remote Sensing of Environment*, 279:113138.

Yang, Y., Long, D., Guan, H., Scanlon, B. R., Simmons, C. T., Jiang, L., and Xu, X. (2014). Grace satellite observed hydrological controls on interannual and seasonal variability in surface greenness over mainland australia. *Journal of Geophysical Research: Biogeosciences*, 119(12):2245–2260.

Yeh, P. J.-F., Swenson, S. C., Famiglietti, J. S., and Rodell, M. (2006). Remote sensing of groundwater storage changes in illinois using the gravity recovery and climate experiment (grace). *Water Resources Research*, 42(12).

Yin, G. and Park, J. (2021). The use of triple collocation approach to merge satellite-and model-based terrestrial water storage for flood potential analysis. *Journal of Hydrology*, 603:127197.

Yoo, C. and Kim, S. (2004). Eof analysis of surface soil moisture field variability. *Advances in Water Resources*, 27(8):831–842.

Zhao, M., Velicogna, I., and Kimball, J. S. (2017). Satellite observations of regional drought severity in the continental united states using grace-based terrestrial water storage changes. *Journal of Climate*, 30(16):6297–6308.

Received: *2023-03-22*

Reviewed: *2023-04-13 (undisclosed name); 2023-04-19 (undisclosed name)*

Accepted: *2023-06-16*